14th International Conference on Structural Safety and Reliability - ICOSSAR'25
1-6 June, 2025 - Los Angeles California, USA
R. Ghanem, E. Johnson, S. Masri and A. Olivier (Eds)

INFRASTRUCTURE WIND RISK ASSESSMENT UNDER CLIMATE CHANGE: AN INTEGRATED ANALYSIS OF METAL ROOFS, POWER NETWORKS AND STREET TREES

CHI-YING LIN*, **YU-KAI CHUANG**, **AND CHENG-EN TSAI**

National Yang Ming Chiao Tung University
No. 1001, Daxue Rd, East District, Hsinchu City, 30010

Emails: chiyinglin@nycu.edu.tw (C.-Y. Lin, Corresponding Author)
ykchuang0225@gmail.com (Y.-K. Chuang);
tsai.en11@nycu.edu.tw (C.-E. Tsai)

Key words: Wind disasters, Vulnerability analysis, Metal roofs, Power networks, Street trees, Monte Carlo simulation, Machine learning, Climate change, Cascading failures

Abstract. Climate change intensifies global extreme weather events, significantly heightening the risks posed by wind disasters to urban infrastructures such as metal roofs, power networks, and street trees. This research develops a comprehensive regional wind risk assessment framework specifically tailored to evaluate the compounded vulnerabilities of these elements under future climate scenarios. Utilizing advanced computational methods, the study assesses metal roofs through deep learning-based satellite image segmentation and machine learning-driven vulnerability modeling. For street trees, structural vulnerabilities are quantified using finite element analysis and AI-based species classification. Power network risks are analyzed using adapted wind vulnerability curves and a network exposure model constructed via Minimum Spanning Tree algorithms. Monte Carlo simulations and wind-driven debris trajectory models further enrich the analysis, capturing cascading failure mechanisms resulting from interactions among infrastructure components. Results indicate significant variability in vulnerability across regions, driven primarily by infrastructure density and wind direction. Particularly, the study demonstrates disproportionate damage increases at higher wind speeds, with regional hotspots clearly identified. Integration of vulnerability curves for each infrastructure component offers quantitative predictions of damage probabilities, thus serving as a robust foundation for climate change adaptation strategies. Ultimately, this integrated analysis provides critical insights into infrastructure interdependencies and highlights specific urban planning and management strategies to enhance resilience against wind-related disasters. Findings support evidence-based decision-making processes and underscore the importance of proactive infrastructure reinforcement and adaptive urban vegetation management in mitigating climate-induced wind disaster risks.

1 INTRODUCTION

Taiwan, situated in the Western Pacific typhoon corridor, faces significant natural disaster risks from typhoons, which pose a growing threat to national security. Statistical data indicates

that an average of four to five typhoons cause substantial damage annually, resulting in property damage and casualties [1]. In the context of global climate change and warming, the El Niño–Southern Oscillation phenomenon and eastward shifting ocean warming are causing typhoon generation locations to move eastward. This shift extends typhoons' paths through Western Pacific coastal regions, potentially increasing their intensity and making their trajectories more unpredictable [2]. Although Taiwan may experience fewer typhoons due to these eastward shifts, the severity of damage from stronger typhoons could be significantly greater when they do occur.

While most buildings in Taiwan are constructed with reinforced concrete or steel structures that generally withstand typhoon winds, non-structural components and auxiliary facilities—such as metal roofs, windows, street trees, solar panels, signage, and construction scaffolding—frequently sustain damage during high winds [3]. These components, despite their seemingly secondary importance to main building structures, often account for a disproportionately high percentage of typhoon damage statistics. For instance, during Typhoon Aere in 2004, fallen street trees alone accounted for 65.15% of reported damage incidents in Taipei City, highlighting the critical vulnerability of these urban landscape elements [3].

Street trees, in particular, can cause significant obstruction to road traffic when they fall. A fallen tree's contact point with the ground can block or obstruct roadways, sometimes entrapping other objects caught in the storm, such as vehicles, cables, or street lamps. Such obstructions create chaos, prevent timely evacuation during emergencies, and impede rescue teams from reaching affected areas quickly, causing potentially irreversible damage to emergency response operations [5]. Furthermore, fallen trees can trigger additional hazards. For example, if a fallen tree strikes power lines, it can cause power outages affecting critical infrastructure operations such as medical facilities, police stations, and fire departments, and potentially ignite fires, exacerbating disaster conditions [5, 6]. Metal roofs represent another highly vulnerable component during typhoons. According to post-disaster investigations, metal roof failures are prevalent during typhoon events. Research has shown that these failures usually stem from connection problems rather than material failures—specifically the pull-through and pull-out failures of screw fasteners connecting metal sheets to supporting structures [7, 8]. These connection failures can lead to metal sheets becoming dangerous wind-borne debris that potentially impacts power lines and other infrastructure. Power networks face dual vulnerability during typhoons—direct damage from wind forces and indirect damage from falling trees or flying debris. When power poles fail due to high winds or collisions with debris, the cascading effects can extend far beyond the immediate damage site due to the networked nature of power distribution systems [9]. The interdependence between these infrastructure components creates complex failure scenarios that require comprehensive assessment frameworks.

Traditional vulnerability assessments often focus on individual infrastructure components in isolation, failing to capture the cascading effects that characterize real-world disasters. An integrated approach is necessary to understand how the failure of one component (e.g., a metal roof or street tree) might impact other critical systems (e.g., power networks or road networks) [10].

The development of an integrated risk assessment framework requires several key components: exposure models that accurately identify and characterize vulnerable elements; mechanical models that predict failure modes under different wind conditions; and impact assessment models that evaluate cascading effects on interconnected infrastructure systems.

Such frameworks increasingly incorporate advanced computational methods, including finite element analysis, machine learning algorithms, and Monte Carlo simulations to handle the inherent uncertainties in both hazard intensities and infrastructure responses [11, 12].

As climate change alters the frequency, intensity, and spatial patterns of typhoons, infrastructure resilience becomes increasingly critical. Research suggests that climate change may lead to fewer but more intense typhoons in the Western Pacific region, potentially increasing the maximum wind speeds experienced during extreme events [2]. This shift necessitates a reevaluation of current design standards and risk assessment methodologies to ensure they remain appropriate for future climate conditions. Studies on infrastructure resilience under climate change scenarios have highlighted the importance of adaptive design strategies, improved maintenance protocols, and robust risk assessment frameworks that can account for changing hazard profiles [12]. These approaches are essential for developing climate-resilient urban environments capable of withstanding increasingly severe wind events.

2 METHODOLOGY

2.1 Exposure Assessment

The exposure assessment employed advanced remote sensing and computational methods to identify and quantify critical infrastructure components in the study area. This comprehensive approach enabled the systematic collection of spatial data for metal roofs, street trees, and power networks, forming the foundation for subsequent vulnerability analysis. For metal roof identification, a U-Net deep learning model was implemented using satellite imagery [5]. The model architecture utilized an encoder-decoder structure with skip connections, processing 256×256 pixel input images. Training data consisted of 45 manually annotated images that were augmented to 900 samples using various techniques, including rotation, flipping, and brightness adjustment. The model achieved a best F1-score of 0.86403 with an optimal threshold of 0.23737, demonstrating robust detection capabilities. Regional analysis identified 2,665 metal roofs in Luodong Township after implementing area-based filtering and integration with 3D building models. Street tree detection employed DeepForest, a specialized deep learning framework based on the RetinaNet architecture [6]. Two model variants were developed: a three-class classification model for species-specific detection and a single-class model focusing on tree detection accuracy. The single-class model demonstrated superior performance with a precision of 0.4215 and a recall of 0.6905. Street trees were categorized into four clusters using the DBSCAN algorithm, based on morphological and mechanical properties (Table 1).

Table 1: Distribution and quantity of classified street tree types

Cluster	Tree type	Amount	Percentage
1	Camphora officinarum、Ficus subg. Urostigma、Koelreuteria elegans ssp. Formosana、Millettia pinnata、Bischofia javanica、Bombax ceiba、Liquidambar formosana、Fraxinus griffithii、Terminalia mantaly、Peltophorum pterocarpum、Roystonea regia、Lagerstroemia speciosa、Ficus religiosa	58765	83.55%
2	Melaleuca	5440	7.73%
3	Alstonia scholaris、Cerasus serrulata	4745	6.75
4	Melia azedarach	1389	1.97%

Power network exposure assessment utilized government-provided distribution data combined with Minimum Spanning Tree (MST) algorithms for network reconstruction [5]. Both Prim's and Kruskal's algorithms were implemented to establish electrical connectivity between 2,592 power poles and a secondary substation. MST-

based network modeling yielded similar results for both algorithms, with average clustering coefficient of 0.0, network density of 0.00077, and average path length of 154.85. The resulting network comprised 2,591 edges connecting the identified power poles, with comprehensive topology information stored in structured databases (Table 2). This exposure assessment methodology provided spatially explicit data for regional vulnerability analysis, enabling precise quantification of infrastructure components and their spatial relationships essential for disaster impact evaluation.

Table 2: Regional exposure statistics for power networks

Network property	Prim's Algorithm	Kruskal's Algorithm
Clustering Coefficient	0.0	0.0
Network Density	0.00077	0.00077
Average Shortest Path Length	154.85117	154.85117
Network Diameter	484	484
Average Degree	1.99923	1.99923
Average Betweenness Centrality	0.05940	0.05940
Branching Factor	1.99923	1.99923

2.2 Structural Vulnerability Analysis

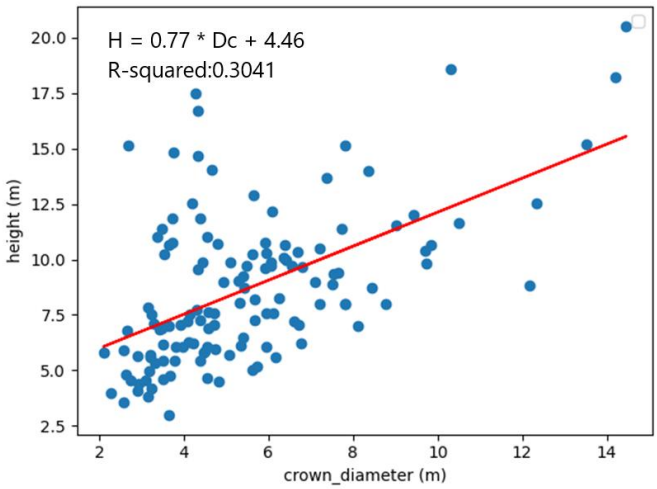

Figure 1: Relationship between tree crown diameter and tree height (first category)

The structural vulnerability analysis employed advanced computational methods to evaluate the resistance capacity of both street trees and metal roofs under wind loading conditions. Two distinct approaches were utilized: finite element method for street trees and machine learning models for metal roofs. Street tree vulnerability was assessed using a mechanical wind loading model based on finite element analysis [6]. Trees were simplified as cantilever beam systems with multiple elements representing trunk segments, each characterized by local coordinate systems and material properties. The model incorporated tree crown and trunk geometries derived from regression analysis of physical measurements (Figure 1), showing strong correlations between crown diameter and tree height across different species clusters.

The FEM model integrated three loading components: wind forces acting on crown and trunk, self-weight effects, and P-Delta effects. Wind loads were calculated using drag coefficients and streaming coefficients accounting for crown deformation at higher wind speeds. Material properties for four tree clusters were established through clustering analysis of 17 representative species (Table 3), with physical parameters including stem density (480.5-740.5 kg/m^3), modulus of rupture (61-137 MPa), and modulus of elasticity (8,649-17,848 MPa). Two failure modes were considered: stem breakage occurring when tensile stress exceeded modulus of rupture, and

uprooting when maximum moment exceeded critical overturning moment Monte Carlo simulation with 50,000 iterations per analysis established fragility curves for different crown diameter ranges (5-10m, 11-15m, 16-20m) across the four tree categories.

Metal roof vulnerability assessment utilized machine learning regression models based on experimental pull-out failure data [5]. Three algorithms were compared: multiple linear regression, Random Forest, and XGBoost. Model inputs included bolt characteristics (thread pitch, diameter), batten thickness, and tensile strength. XGBoost demonstrated superior performance with $R^2 = 0.976$ after hyperparameter optimization (max_depth = 2, n_estimators = 86, learning_rate = 0.41). The model processed 170 experimental data points across 19 bolt types and 12 batten configurations. The trained model calculated single bolt capacity, which was then converted to unit area capacity by incorporating bolt density patterns (6.67-13.33 bolts/m²) typical of local installation practices.

Monte Carlo simulation with 5,000 iterations established regional fragility curves for Luodong Township, incorporating randomness in material properties (COV = 0.1-0.15) and geometric parameters. Results indicated that metal roofs exhibited greater resilience compared to street trees, with significant damage occurring only at higher wind speeds.

Table 3: Physical and mechanical properties of various street tree species

Tree Type	Density (kg/m3)	modulus of rupture (MPa)	Young's modulus (MPa)
Camphora officinarum	1000	99.734	10483.3
Ficus subg. Urostigma	441	82.3759	13042.8445
Koelreuteria elegans ssp. Formosana	595	100.7143	12679.998
Millettia pinnata	619.8	116.1107	12258.313
Bischofia javanica	1067	96	12062.1795
Bombax ceiba	320.5	82.3759	13042.8445
Melaleuca	740.5	137.2931	17848.103
Alstonia scholaris	397.3	61.5858	8521.9788
Cerasus serrulata	563.7	58.7418	8776.9518
Liquidambar formosana	1000	110.9132	12679.9984
Fraxinus griffithii	1106	103.3621	10855.9615
Terminalia mantaly	569	95.5168	10022.396
Peltophorum pterocarpum	602.5	116.1107	12258.313
Roystonea regia	660.2	116.1107	12258.313
Melia azedarach	900	61	10689.2485
Lagerstroemia speciosa	632.5	132.3898	14200.029
Ficus religiosa	443	82.3759	13042.8445

2.3 Cascading Impact Analysis

A comprehensive debris trajectory model was developed to analyze the potential impact of failed structural elements on urban infrastructure [5]. This model incorporated both metal roof debris and fallen street trees, employing differential equations to simulate trajectory paths under varying wind conditions.

For plate-type debris (metal roofs), the trajectory analysis utilized modified aerodynamic equations from [13] and [14]. The model considered key parameters including drag coefficients, lift coefficients, moment coefficients, and streaming coefficients that varied with wind speed and attack angle. The governing equations incorporated three coupled differential equations for horizontal displacement, vertical displacement, and rotational motion.

The trajectory model accounted for random parameters through statistical distributions: initial attack angle (normal distribution: $\mu = 5.35°$, $\sigma = 1.34°$), plate thickness (uniform sampling from 0.37-0.52mm), and material density (uniform distribution: 7,750-8,050 kg/m³). A surrogate model was developed using XGBoost regression, trained on 2,376 trajectory simulations across various wind speeds and relative heights (Figure 2). The surrogate model achieved $R^2 = 0.98$, enabling rapid prediction of horizontal displacement and standard deviation based on wind speed and relative height inputs.

For street tree trajectories, the model simplified trees as rigid bodies with asymmetric fall patterns influenced by crown mass distribution and terrain effects. Tree fall direction was determined by wind direction, with

consideration for topographic shielding effects and surrounding vegetation.

Monte Carlo simulations formed the core methodology for developing vulnerability curves across all infrastructure components. The simulation framework involved systematic parameter sampling from probability distributions to capture inherent uncertainties in material properties, geometric configurations, and environmental conditions. For metal roofs, 5,000 Monte Carlo iterations were conducted for each wind speed, incorporating random selection of bolt properties, installation patterns, and material characteristics. Convergence analysis demonstrated that results stabilized within ±1% variance at this simulation count.

Street tree simulations utilized 50,000 iterations per analysis based on convergence studies. Random variables included tree geometry (following cluster-specific regression relationships), material properties (species-dependent distributions), and wind loading parameters. The simulation framework generated failure probability data across wind speed ranges (10-90 m/s), accounting for multiple failure modes: metal roof pull-through and pull-out failures, tree stem breakage, and uprooting. Results were processed to develop cumulative distribution functions representing vulnerability curves for each infrastructure category.

Integration of debris trajectory simulations with infrastructure vulnerability enabled assessment of secondary impacts. The model evaluated collision probabilities between airborne debris and critical systems, incorporating geometric constraints and impact thresholds to determine failure cascades affecting power networks and road systems.

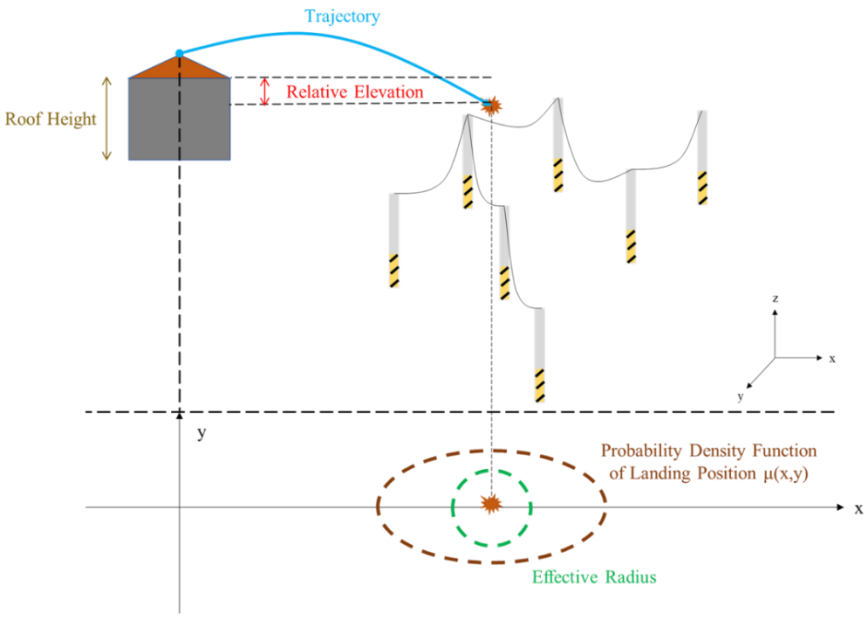

Figure 2: Schematic of wind-driven debris trajectory prediction model

3 RESULTS AND DISCUSSION

3.1 Component Vulnerability

The vulnerability analysis established comprehensive vulnerability curves for three critical infrastructure components: metal roofs, street trees, and power networks in the Luodong region. Each component demonstrated distinct failure patterns and thresholds under increasing wind speeds.For metal roofs, the vulnerability curves revealed that structural failure predominantly occurred through pull-out failures of screw connections rather than material strength limitations [8, 15]. The analysis utilized experimental data from pull-out failure tests and employed XGBoost regression models to predict individual screw capacity, achieving an R^2 value of 0.976. Figure 3 illustrates the regional vulnerability curves for Luodong's metal roofs, showing minimal failure probability below 35 m/s wind speeds, with exponential increases thereafter. The curves demonstrate increasing failure rates from

approximately 0.07% at 33.1 m/s to over 90% beyond 60 m/s wind speeds. Validation against historical typhoon data, specifically the 2004 Typhoon Aere impacts on Taipei, confirmed the model's accuracy, with predicted failure rates falling within the range of actual reported damages [5].

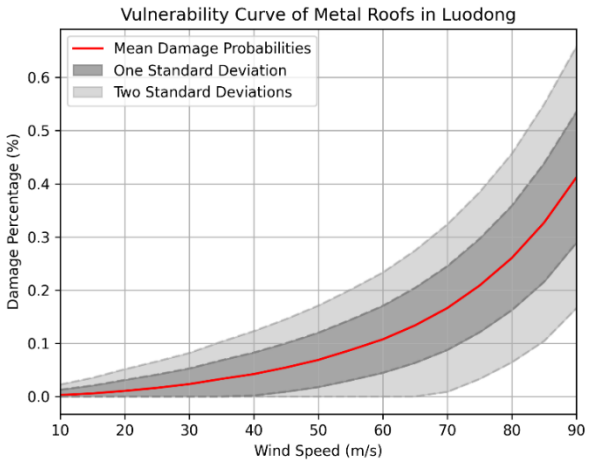

Figure 3: Vulnerability curves for metal roofs in Luodong region

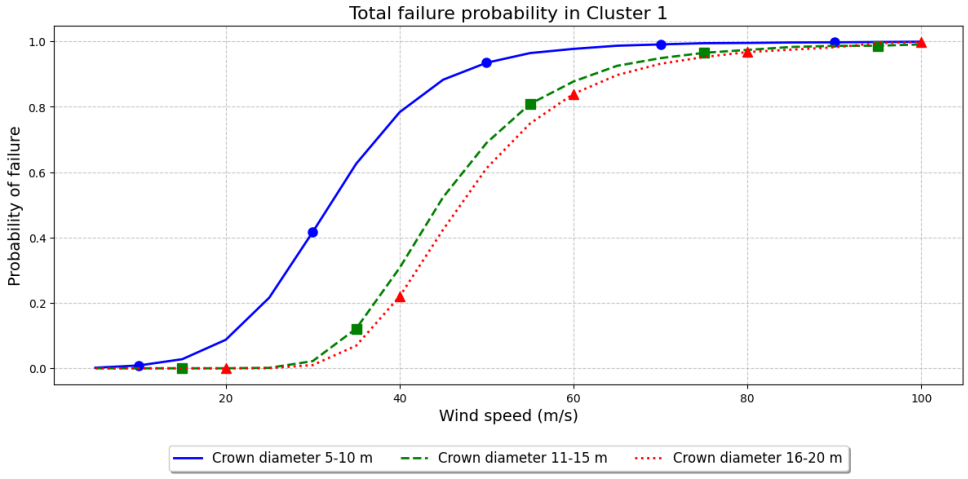

Figure 4: Vulnerability curves for street trees (primary category)

Street tree vulnerability analysis employed finite element modeling combined with Monte Carlo simulation to establish failure curves for four tree categories [10]. The analysis considered both stem breakage and uprooting failure modes, with critical parameters including tree height, crown diameter, and wood mechanical properties. Figure 4 presents the vulnerability curves for the primary tree category, revealing that trees with larger crowns (16-20m) demonstrated superior wind resistance compared to smaller specimens (5-10m crowns). The figure shows failure probabilities remain below 10% until approximately 40 m/s, then increase dramatically to over 90% at 50 m/s. The curves indicate that failure typically initiated at tree bases, with larger crown diameters correlating with increased structural stability [6].

Power network vulnerability incorporated both individual pole failure and cascading effects through the distribution network topology [16]. The analysis utilized concrete pole fragility curves from previous research [17], adjusted for local terrain and elevation factors. Figure 5 demonstrates that power network vulnerability in Luodong exhibited rapid escalation beyond 45 m/s wind speeds, with nearly complete network failure predicted

at 70 m/s. The vulnerability curves show minimal failure below 30 m/s, increasing to approximately 50% at 45 m/s, and approaching 100% at 60 m/s. The analysis accounted for power supply chain relationships, demonstrating how upstream failures propagated through downstream segments, amplifying regional impact [18].

Comparative analysis revealed significant differences in component resilience. Metal roofs exhibited the highest wind resistance, maintaining structural integrity until approximately 50 m/s wind speeds. Street trees showed intermediate vulnerability, with failure patterns varying by species category and size characteristics. Power networks demonstrated the lowest resilience, becoming critical failure points at moderate wind speeds due to their interconnected nature.

The vulnerability curves incorporated statistical variations through standard deviation bounds, acknowledging uncertainties in material properties, wind loading patterns, and structural configurations. Monte Carlo simulations with convergence analysis ensured statistical reliability, with simulation counts ranging from 5,000 to 50,000 iterations depending on component complexity [11]. These findings align with historical damage patterns from typhoon events in Taiwan, where infrastructure failures primarily affect non-structural components and utility systems rather than primary building structures [3]. The established vulnerability curves provide essential input for regional risk assessment and disaster preparedness planning in typhoon-prone regions.

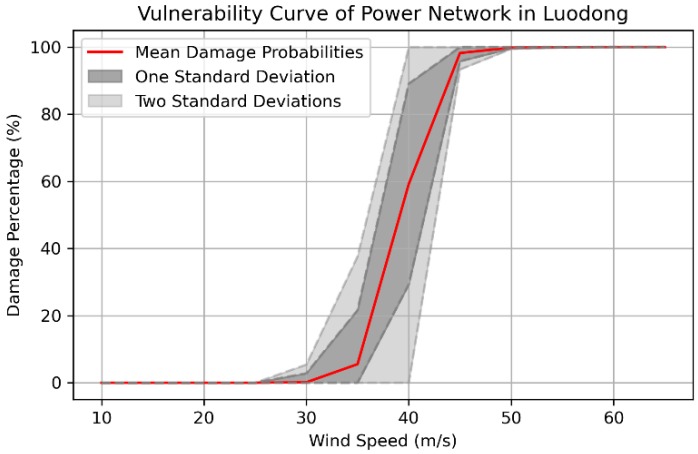

Figure 5: Power network vulnerability analysis results in Luodong region

3.2 Cascading Failures

The cascading failure analysis revealed significant secondary impacts from infrastructure debris on critical urban systems. The research examined two primary pathways: metal roof debris impacts on electrical networks and street tree failures affecting both road and power infrastructure.

Metal roof debris trajectories were modeled using plate-type windborne debris equations [13], considering both streamwise and crosswind displacement patterns. The analysis incorporated debris trajectory prediction models that accounted for roof dimensions, wind speed, and release conditions. Figure 6 demonstrates the spatial distribution of potential power network damage caused by metal roof debris under northerly wind conditions (0° wind direction). The simulation revealed that metal roof failures could cause significant collateral damage to overhead power lines, with impact probabilities increasing substantially at wind speeds above 50 m/s. The model utilized three-dimensional trajectory analysis, incorporating statistical variations in debris fall patterns to predict cable contact probabilities. However, when overlaying these results with direct wind-induced power network failures, the additional impact from flying debris was relatively minimal compared to the primary wind damage to utility poles.

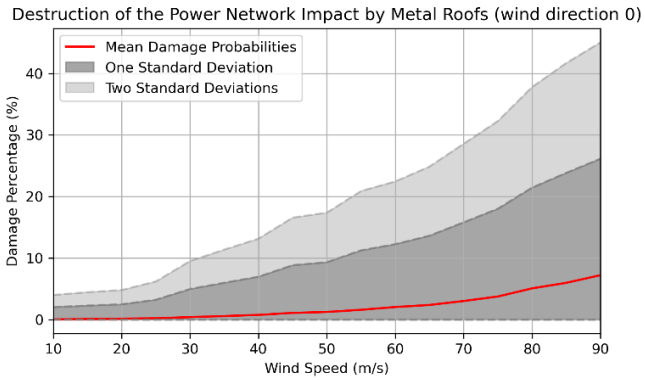

Figure 6: Collateral damage to power network caused by metal roof debris (wind direction 0°)

Street tree failures presented more complex cascading effects on regional infrastructure. The analysis employed detailed geometric relationships to determine road obstruction patterns, defining a road segment as blocked when the remaining passable width fell below 2.5 meters after tree failure. Figure 7 illustrates the proportion of road network disruption under northeast wind conditions (45° wind direction) using a three-category tree model. The results indicated that road blockage rates increased exponentially with wind speed, reaching approximately 15% at 50 m/s and exceeding 30% at 60 m/s. The analysis incorporated tree fall direction predictions based on wind vectors, accounting for tree morphology and root system characteristics.

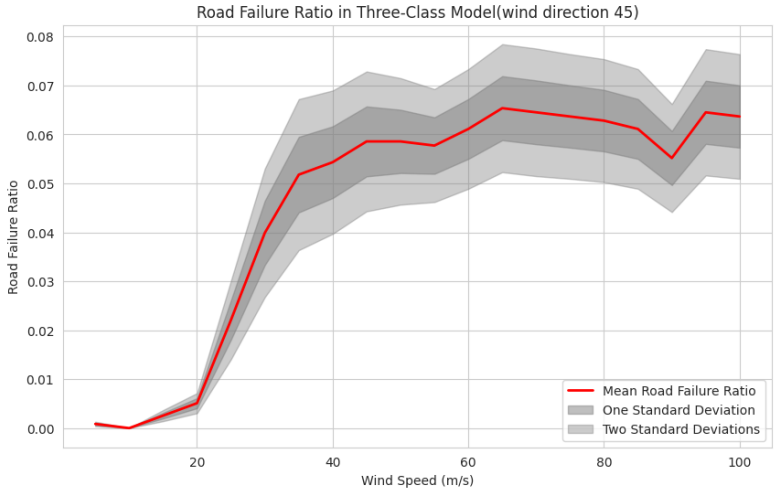

Figure 7: Proportion of road network disruption due to fallen street trees (wind direction 45°)

Regarding power network impacts, street tree failures demonstrated significant cascading potential through direct cable contact and subsequent upstream-downstream network dependencies. Figure 8 presents the collateral damage assessment for the electrical distribution system under the same northeast wind conditions. The vulnerability analysis incorporated minimum spanning tree algorithms [16] to model power distribution topology, enabling tracking of failure propagation through the network hierarchy. Results showed that while individual tree-cable contact events occurred at relatively low rates (under 5% at moderate wind speeds), the interconnected nature of the power distribution system amplified these localized failures into broader regional outages.

The cascading analysis revealed distinct patterns across different wind directions. Northeast and southwest winds (45° and 225°) consistently produced higher failure rates due to the spatial alignment of infrastructure elements. For road networks, these conditions resulted in 20-30% higher blockage rates compared to other wind

directions at equivalent wind speeds. Power network cascading impacts showed similar directional sensitivity, with collateral damage rates varying by up to 40% depending on wind orientation.

Critical differences emerged between the impacts of metal debris versus tree failures. Metal roof debris demonstrated high individual impact potential but affected limited spatial areas. Conversely, street tree failures exhibited lower individual impact intensities but broader spatial distribution, creating more extensive cascading effects across both transportation and power networks. The analysis revealed that power networks were particularly vulnerable to cascading failures due to their linear topology and upstream-downstream dependencies, with single failures potentially affecting hundreds of downstream customers. The cascading failure assessment incorporated uncertainty through Monte Carlo simulations with 3,000 iterations, ensuring statistical reliability while maintaining computational efficiency. Sensitivity analysis indicated that small variations in wind direction (±15°) could alter total network impact by up to 25%, emphasizing the importance of considering directional effects in regional vulnerability assessments.

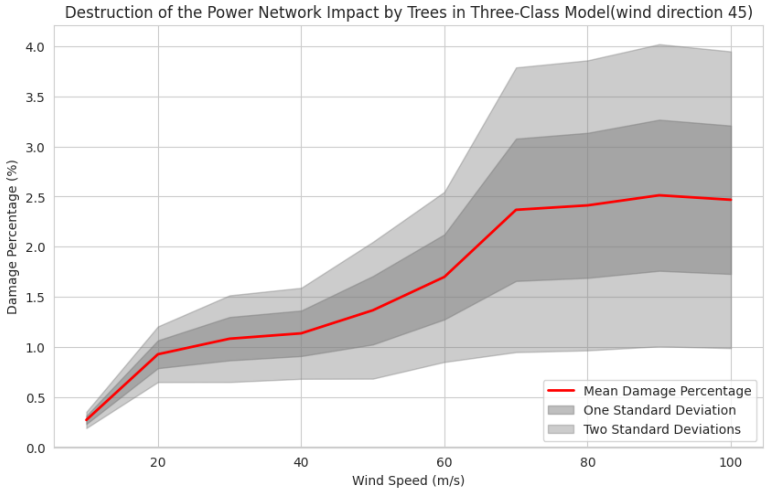

Figure 8: Proportion of collateral damage to power network due to street tree failure (wind direction 45°)

4 CONCLUSIONS

This study developed comprehensive vulnerability assessment frameworks for urban non-structural infrastructure components under typhoon conditions, with specific applications to metal roofs, street trees, power networks, and road systems. The analysis of historical disaster records from multiple typhoon events confirmed that non-structural components represent the primary source of typhoon damage in Taiwan, constituting over 65% of total disaster incidents. The metal roof vulnerability assessment incorporated machine learning techniques, achieving high predictive accuracy ($R^2 = 0.976$) using XGBoost algorithms combined with deep learning U-Net models for spatial distribution mapping. Monte Carlo simulations with 5,000 iterations established vulnerability curves showing failure probabilities ranging from minimal at 30 m/s to near-complete at 80 m/s wind speeds. Power network analysis revealed that direct wind impacts far exceeded collateral damage from metal roof failures, with critical vulnerability thresholds at 50-55 m/s wind speeds. Street tree research employed finite element analysis using direct stiffness methods, classifying 17 species into four categories based on physical properties. Vulnerability analysis demonstrated that larger trees (16-20m canopy diameter) in Categories 1 and 2 exhibited superior wind resistance, while Category 3 trees showed increased vulnerability with size. Road blockage analysis indicated that northeastern and southwestern winds created the highest obstruction risks, with critical failure occurring when residual road width decreased below 2.5 meters.

The findings provide actionable insights for enhancing Taiwan's disaster preparedness infrastructure. Priority should be given to power network reinforcement, particularly for utility poles that demonstrate critical vulnerabilities at moderate wind speeds (45-50 m/s). The minimal impact of metal roof failures on power networks suggests that direct pole strengthening represents the most effective intervention strategy. Urban planning guidelines should incorporate vulnerability-based zoning, with high-risk areas identified through the developed

assessment models receiving enhanced infrastructure protection. Road network design must account for tree-related blockage risks, particularly in corridors aligned with prevailing typhoon wind directions. The establishment of minimum clearance standards (2.5-meter residual width) provides a quantitative basis for road design specifications. Street tree management strategies should adopt species-specific approaches, with Category 3 and 4 trees requiring more intensive maintenance schedules and strategic positioning away from critical infrastructure. Pre-typhoon preparation protocols should prioritize tree trimming based on empirically-derived vulnerability classifications rather than uniform management approaches.

This research advances disaster vulnerability assessment methodologies by integrating machine learning, deep learning, and Monte Carlo simulation techniques within a unified framework. The development of vulnerability curves for specific geographic contexts (i.e., Luodong Township) demonstrates scalability potential for broader regional applications. However, limitations include reliance on historical data that may not fully capture future climate change impacts, and assumptions regarding soil conditions and tree root systems that require site-specific validation. The study's focus on two specific locations provides valuable case studies but necessitates careful consideration when extrapolating findings to other regions with different topographic, climatic, or infrastructure characteristics. Future research should expand the geographical scope and incorporate real-time meteorological data integration for dynamic vulnerability assessment.

Policy-makers should prioritize the implementation of risk-based infrastructure standards, drawing from the quantitative vulnerability thresholds established in this study. Building codes should incorporate enhanced metal roof attachment specifications derived from experimental data, while urban forestry policies must integrate species vulnerability classifications into public space planning guidelines. Integration with Taiwan's National Disaster Prevention Framework requires developing automated vulnerability assessment systems that combine meteorological forecasts with infrastructure databases. This technological advancement would enable predictive maintenance scheduling and optimize emergency resource allocation during typhoon events. Future research priorities include: (1) expanding the assessment framework to additional non-structural components such as signage, scaffolding, and water storage systems; (2) incorporating climate change projections into vulnerability models to account for increasing typhoon intensity; (3) developing economic impact assessment tools to support cost-benefit analyses of infrastructure hardening investments; and (4) establishing real-time monitoring networks for continuous vulnerability assessment and early warning capabilities.

This research contributes to the growing body of knowledge on urban disaster resilience by providing quantitative tools for infrastructure vulnerability assessment. The methodologies developed can be adapted for application in other typhoon-prone regions, supporting international disaster risk reduction efforts. By establishing empirical relationships between meteorological conditions and infrastructure failure probabilities, this study bridges the gap between engineering analysis and practical disaster management policy. The findings underscore the critical importance of comprehensive vulnerability assessments that consider cascading failure mechanisms across interconnected urban systems. As climate change intensifies extreme weather events, the frameworks developed in this research provide essential tools for building more resilient communities and informing evidence-based policy decisions for disaster risk reduction in the Asia-Pacific region.

REFERENCES

[1] Huang, W. K., & Wang, J. J. (2015). Typhoon damage assessment model and analysis in Taiwan. Natural Hazards, 79(1), 497-510.

[2] IPCC. (2013). Climate change 2013 the physical science basis: Working Group I contribution to the fifth assessment report of the intergovernmental panel on climate change (T. F. Stocker, D. Qin, G.-K. Plattner, M. Tignor, S. K. Allen, J. Boschung, A. Nauels, Y. Xia, V. Bex, & P. M. Midgley, Eds.). Cambridge University Press. https://doi.org/10.1017/CBO9781107415324

[3] Chien, C. W., & Jang, J. J. (2008). Case study of wind-resistant design and analysis of high mast structures based on different wind codes. Journal of Marine Science and Technology, 16(4), 6.

[4] Leung, Z.-W. (2018). Studies on casual factors and their management of tree falling by

typhoon at Taipei areas [Master's thesis, National Taiwan University]. https://doi.org/10.6342/NTU201801375

[5] Chuang, Y.-K. (2023). Regional risk assessment of metal roofs and power networks in wind disasters [Master's thesis, National Yang Ming Chiao Tung University]. https://hdl.handle.net/11296/ayx52u

[6] Tsai, C.-E. (2025). Vulnerability analysis of street trees under wind hazards and their impact assessment on road and power network [Master's thesis, National Yang Ming Chiao Tung University]. https://hdl.handle.net/11296/2k5xhp

[7] Sivapathasundaram, M., & Mahendran, M. (2016). Experimental studies of thin-walled steel roof battens subject to pull-through failures. Engineering Structures, 113, 388-406.

[8] Sivapathasundaram, M., & Mahendran, M. (2018). New pull-out capacity equations for the design of screw fastener connections in steel cladding systems. Thin-Walled Structures, 122, 439-451.

[9] Mu, Y., Li, L., Hou, K., Meng, X., Jia, H., Yu, X., & Lin, W. (2022). A risk manage-ment framework for power distribution networks undergoing a typhoon disaster. IET Generation, Transmission & Distribution, 16(2), 293-304.

[10] Hou, G., & Chen, S. (2020). Probabilistic modeling of disrupted infrastructures due to fallen trees subjected to extreme winds in urban community. Natural Hazards, 102, 1323-1350.

[11] Konthesingha, K. C., Stewart, M. G., Ryan, P., Ginger, J., & Henderson, D. (2015). Reliability based vulnerability modelling of metal-clad industrial buildings to extreme wind loading for cyclonic regions. Journal of Wind Engineering and Industrial Aerodynamics, 147, 176-185.

[12] Stewart, M. G., Ginger, J. D., Henderson, D. J., & Ryan, P. C. (2018). Fragility and climate impact assessment of contemporary housing roof sheeting failure due to ex-treme wind. Engineering Structures, 171, 464-475.

[13] Holmes, J. D., Letchford, C. W., & Lin, N. (2006). Investigations of plate-type windborne debris—Part II: Computed trajectories. Journal of Wind Engineering and Industrial Aerodynamics, 94(1), 21-39.

[14] Tachikawa, M. (1983). Trajectories of typhoon-generated missiles. Wind Engineers, JAWE, 1983(17), 21-30.

[15] Sivapathasundaram, M., & Mahendran, M. (2017). Numerical studies and design of thin steel roof battens subject to pull-through failures. Engineering Structures, 146, 54-74.

[16] Montoya, D. P., & Ramirez, J. M. (2012, July). A minimal spanning tree algorithm for distribution networks configuration. In 2012 IEEE Power and Energy Society General Meeting (pp. 1-7). IEEE.

[17] Mu, Y., Li, L., Hou, K., Meng, X., Jia, H., Yu, X., & Lin, W. (2022). A risk management framework for power distribution networks undergoing a typhoon disaster. IET Generation, Transmission & Distribution, 16(2), 293-304.

[18] Shengqiang, Z., Yifeng, H., Jianlong, C., & Junwu, W. (2018, November). A new method based on Monte Carlo simulation for reliability evaluation of distribution network considering the influence of typhoon. In 2018 International Conference on Power System Technology (POWERCON) (pp. 3341-3346). IEEE.

[19] Lin, N., & Vanmarcke, E. (2010). Windborne debris risk analysis—Part I. Introduction and methodology. Wind and Structures, 13(2), 191.